Superalloys 2004
Edited by K.A. Green, T.M. Pollock, H. Harada,
T.E. Howson, R.C. Reed, J.J. Schirra, and S. Walston
TMS (The Minerals, Metals & Materials Society), 2004

MICROSTRUCTURAL STABILITY AND CREEP OF Ru-CONTAINING NICKEL-BASE SUPERALLOYS

L.J. Rowland, Q. Feng, and T.M. Pollock
University of Michigan, Dept. of Materials Science and Engineering
Ann Arbor, MI 48109

Keywords: creep, single crystal, Ruthenium, γ-γ' lattice misfit, γ' precipitate morphology

Abstract

Nickel-base single crystal superalloys with Ru additions of 5.7 to 9.7 wt%, moderate amounts of refractory elements and up to 6.7 wt% Cr were investigated. The γ' precipitate morphology of the experimental alloys was cuboidal, near-spherical and intermediately-shaped depending on the Cr and Ru content. The time to 1% creep and the creep rupture lives of the experimental alloys were measured at 950°C and 290 MPa. Within the set of alloys investigated rafting occurred parallel to the axis of the applied uniaxial tensile stress, perpendicular to the applied stress or was completely suppressed, suggesting a wide range of lattice misfit. Interfacial dislocation network development during creep also varied widely among the alloys investigated. The possibilities for control of microstructure and high temperature properties via Ru additions are discussed.

Introduction

There is a continuing demand for development of nickel-base superalloys that can maintain structural integrity at temperatures of 1100°C and beyond. Ru additions have been found to increase the liquidus temperature of Ni-Al-Ru ternary alloys [1] and nickel-base superalloys [2]. Early studies on the addition of Ru to single crystal nickel-base superalloys reported a reduced propensity for formation of topologically close-packed (TCP) phases and improved creep rupture strength at 1100°C [3]. Additional investigations have verified a lower tendency for formation of TCP phases [1, 4, 5] and an improved creep resistance at 1100°C in alloys containing 2 to 5 wt% Ru [4, 6]. The mechanisms by which Ru additions improve high temperature microstructural stability are still not well understood [3-5].

To improve high temperature mechanical properties, increasing amounts of refractory elements have been added for solid solution strengthening [7]. Increased alloying with Re and W has resulted in superalloys with a negative γ-γ' lattice misfit, due to the strong partitioning behavior of these elements to the γ phase [7]. There has been much discussion in the literature regarding the relationship between the γ-γ' lattice misfit and the creep resistance of superalloys [8-11]. Though superalloys with a more negative misfit have generally been observed to be more creep resistant, a balance of properties, including solid solution strengthening of the matrix and strength of the γ' are also important [12].

During high temperature deformation of commercial nickel-base superalloys, preferential dislocation glide in the matrix channels occurs with initial deposition of dislocations along the horizontal γ-γ' interfaces for loading in tension. Following this, directional coarsening of the γ' precipitates perpendicular to the applied tensile stress occurs. Concurrently, interfacial dislocation networks evolve to configurations that more efficiently relieve the misfit strain between the precipitate and matrix. The γ-γ' interface, the dislocation network and solid solution strengthening of the matrix impede dislocation motion during the early stages of creep. After rafts form, further deformation requires the dislocations to shear the γ' rafts and the resistance of the γ' to shearing becomes exceedingly important.

Partitioning of elements between the γ and the γ', the γ-γ' lattice misfit, and the precipitate shape are all interrelated. Altering the partitioning behavior of elements such as Re, W and Ta may change the magnitude of the lattice misfit. Precipitates in an alloy with a near-zero misfit will be spherical in the aged condition. If misfit significantly deviates from zero in either the positive or negative direction then the precipitates assume a cuboidal shape [13]. Therefore changes in the γ-γ' phase equilibrium (and therefore elemental partitioning), may change the γ-γ' lattice misfit and the precipitate morphology in both aged and crept material.

There are several possibilities for the mechanisms by which Ru additions may influence high temperature microstructural stability. First, Ru additions may substantially alter the thermodynamics of the superalloy system, decreasing the driving force for precipitation of undesirable phases such as the σ, P, μ and R phases. Conversely other new phases may appear in equilibrium with the γ and the γ' phases at high temperatures; this is the subject of a companion paper in this volume [14]. If the γ-γ' phase equilibrium is modified, partitioning of elements to the phases may be altered, resulting in changes in the γ-γ' lattice misfit and precipitate morphology. O'Hara et al. [3] have reported that Ru additions alter the γ-γ' partitioning behavior, causing Re, W, and Cr to partition less severely to the matrix in superalloys with 0 to 3 wt% Ru. Murakami and coworkers [4] and Yokokawa and coworkers [15] report that 1.46 wt% Ru does not significantly affect the partitioning behavior in TMS-75. Ru additions may also alter the liquidus and solidus temperatures [1, 2] or diffusion kinetics and therefore affect the coarsening rate and creep behavior.

To date, investigations of Ru-containing nickel-base superalloys have considered a relatively narrow range of composition [5, 6] with Ru additions of up to 3 wt% [3, 5, 6]. Additionally, the improvements in creep rupture life of Ru-containing superalloys that have been reported are at and/or above 1100°C [3, 4, 6]. Caron reported improved creep resistance of Ru-containing

nickel-base superalloys at 1150°C, but not at 950°C [4]. No other investigations of the creep behavior of Ru-containing nickel-base superalloys at temperatures below 1100°C have been published to our knowledge.

The objective of this study was to investigate thirty alloys with a wide range of composition and Ru content up to 9.7 wt%. The experimental alloys contained moderate amounts of Re and W. The microstructural phase stability and creep behavior at 950°C have been studied. In addition, preliminary TEM investigations of the dislocation substructures, after approximately 1% creep strain have also been conducted.

Experimental Procedure

Thirty experimental alloys containing from 4.1 to 9.7 wt% Ru, a total of 7.5 to 8.5 wt% of Re and W, and up to 6.7 wt% Cr were investigated. The alloys were cast into polycrystalline ingots by Sophisticated Alloys, Inc. After differential thermal analysis (DTA) and preliminary analysis of solution treated and aged microstructures, selected alloy compositions were cast into single crystal bars. The nominal compositions of the investigated single crystal alloys in this paper are given in Table I.

The single crystal bars were cast in clusters of four (19 mm and 12.7 mm in diameter) in a laboratory-scale Bridgman furnace that accommodates investment molds 15.2 cm in diameter and 30.5 cm in height. A withdrawal rate of 3.3 mm/min from the hot zone was used for all the castings. Following solidification the excess mold material was removed and the surfaces of the bars were lightly polished before macroetching. A hot macroetch bath containing 8 ml HCl, 16 g $FeCl_3$, 11 ml H_2O, and 2 ml HNO_3 was used to check for solidification defects on the surface of the single crystal bars. All the single crystal bars were within 10° of the [001] orientation.

The single crystal bars were solution treated and then aged at 1100°C for 8 hours. The solutioning temperature of each alloy was selected based on the results of DTA scans. The volume fraction of eutectic remaining after solution treatment was less than 5 vol.% in all alloys. Etching specimens with a solution of 33% CH_3COOH, 33% H_2O, 33% HNO_3, and 1% HF revealed the solution treated and aged γ-γ' microstructure. The microstructure was observed using an optical microscope and an XL30 FEG scanning electron microscopy (SEM). A backscattering detector (BSE) was used to differentiate between the dendritic and interdendritic regions. The volume fraction of γ' was determined from both regions using the standard point count method.

After solution treatment and aging, button-head creep specimens were machined by low stress grinding. Vacuum creep testing of [001] oriented creep specimens was performed at 950°C and 290 MPa. The creep conditions were selected to achieve approximately a 1% creep strain in CMSX-4 in 200 hours [16]. After the 200 hour test, the creep specimens were cooled under load to prevent static recovery of dislocations. Creep rupture testing was also performed at 950°C and 290 MPa on select alloys.

After high temperature deformation, material from the button-head and the gage section of creep specimens was sectioned along a plane perpendicular to the applied stress axis with an Isomet slow speed saw. The samples were polished and etched to reveal the orientation of the dendrites, which were used to cut the specimens along a [100] direction parallel to the applied stress axis. The transverse and longitudinal faces from both the button-head and gage sections were imaged in the SEM to observe the post-crept γ-γ' microstructure. Again, a BSE detector was used to differentiate between the dendrites and the interdendritic region. An equivalent procedure was followed for uncrept specimens for comparison.

Transmission electron microscopy (TEM) foils were sectioned from the gage section of crept specimens strained to approximately 1% in 200 hours. The slices were mechanically ground to 175-200 μm using a polishing wheel, and then polished by hand to 100 μm. The final step was jet polishing in a solution of 340 ml methanol, 50 ml percholoric acid, 45 ml distilled water and 65 ml butyl cellusolve. The optimum polishing conditions were determined to be approximately 20 V, 50 mA, and -40°C. A Phillips CM12 Scanning Transmission Electron Micrscope (TEM) with a Gatan modified Phillips Double-Tilt specimen holder was used for analysis of the dislocation substructure. Three invisibility conditions where required for identifying a Burgers vector using the $\mathbf{g}\cdot\mathbf{b}=0$ invisibility criterion.

Table I. Chemical Composition and Liquidus of Experimental Single Crystal Ru-Containing Superalloys (wt%)

Alloy	Ni	Al	Ru	Ta	Re	W	Co	Cr	Liquidus (°C)
UM-F9	bal.	6.1	**9.6**	6.5	3.8	4.4	7.0		1438
UM-F11	bal.	6.0	**9.5**	8.5	3.8	4.3	6.9		1427
UM-F16	bal.	6.2	**9.7**	6.5	3.9	4.4	7.1	**6.7**	1404
UM-F18	bal.	6.0	**5.7**	8.0	4.5	2.9	7.1		1431
UM-F19	bal.	6.0	**5.7**	8.1	4.5	3.0	7.2	**6.7**	1398
UM-F20	bal.	6.0	**5.7**	8.1	4.5	3.0	2.4	**6.7**	1400
UM-F22	bal.	6.0	**5.7**	8.0	4.5	3.0	2.4	**3.4**	1415
UM-F27	bal.	5.9	**5.6**	7.9	7.4	2.9	2.3	**6.6**	1404
UM-F30	bal.	6.0	**5.7**	8.0	4.5	3.0	10.0	**6.7**	1398

Results

No solidification defects were observed on the bars following single crystal solidification. The primary dendrite arm spacing of the experimental alloys cast into single crystals ranged from 300 to 330 μm. It is interesting to note liquidus temperatures are as high as 1438°C and that increasing the Cr content lowers the liquidus temperature of the experimental alloys (Table I). The addition of 6.7 wt% Cr in UM-F16, UM-F19, UM-F20, UM-F27, and UM-F30, results in a decrease of the liquidus temperature by approximately 30°C. Also, UM-F22 with an intermediate amount of Cr (3.4 wt%), had a liquidus temperature of 1415°C.

Precipitate Morphology

After solution treatment and aging, dramatic variation in the γ-γ' microstructures of the experimental alloys was observed. The γ' precipitate morphology in each of the experimental alloys could be characterized as cuboidal, spherical, or intermediately-shaped for both the dendrite core and the interdendritic regions (Table II). The precipitates were considered cuboidal if they had planar interfaces and sharp corners (Figure 1), intermediately-shaped if they displayed planar interfaces with rounded corners (Figure 2) and spherical if they had no planar interfaces or corners (Figure 3). Further discussion of the precipitate morphology in this paper refers to the precipitate morphology within the dendrite core for a given alloy. The volume fraction of γ' in the dendrite core and the interdendritic region is also given in Table II.

It is important to note that all the experimental alloys have a total of 7.5 to 8.3 wt% Re and W. In spite of this relatively high refractory alloy content, near-spherical and intermediately-shaped γ' precipitates were observed. This is in contrast to all current commercial alloys with similar levels of Re and W, where cuboidal precipitates are always present. Cuboidal γ' precipitates were observed in five of the alloys considered in this paper: UM-F16, UM-F19, UM-F20, UM-F27 and UM-F30 (Figure 1a, d, g, j). UM-F18 and UM-F22 had intermediately-shaped γ' precipitates including (Figure 2a, d) and UM-F9 and UM-F11 had spherical γ' precipitates (Figure 3a, d).

In addition to the influence of Ru, the γ' precipitate shape appeared to be strongly dependent on the Cr content. In alloys without Cr the precipitates were spherical, while in alloys with 6.7 wt% Cr the precipitates were strongly cuboidal. The two alloys with intermediately-shaped γ' precipitates, UM-F18 and UM-F22, had 5.7 wt% Ru and no Cr and 5.7 wt% Ru and 3.4 wt% Cr, respectively. Additionally, the Co and Ta levels do not appear to influence the precipitate morphology within the range of compositions investigated.

Creep Behavior and Post-Crept Microstructures

The creep behavior at 950°C and 290 MPa of the [001]-oriented single crystal alloys was also highly variable (Figure 4). While no instabilities with respect to precipitation of TCP phases were observed, there was substantial variation in the directional coarsening behavior of the γ' precipitates. The alloys with cuboidal γ' precipitates (UM-F16, UM-F19, and UM-F20) displayed similar creep behavior in a 200 hour test. They were more creep resistant at 290 MPa and 950°C than the alloys with non-cuboidal precipitate shapes. The two alloys with intermediately-shaped precipitates, UM-F18 and UM-F22, which only varied in their Cr and Co content, displayed vastly different creep behavior from one another at 290 MPa and 950°C. Neither was as creep resistant as the alloys with cuboidal precipitates, though the UM-F22 alloy was significantly more creep resistant than the UM-F18 alloy and the alloys with spherical γ' precipitates.

In Figure 5 the creep curves of UM-F19 and UM-F20 are plotted on an expanded scale. The creep curves of UM-F27 and UM-F30 are also included. The UM-F30 alloy was significantly more creep resistant than the other experimental alloys. At 290 MPa and 950°C the minimum creep rate of UM-F30 was approximately 10^{-10}/sec, an order of magnitude less than the minimum creep rate of UM-F19 and UM-F20, at 10^{-9}/sec.

The creep rupture behavior of the UM-F20 and UM-F27 alloys is shown in Figure 6. UM-F27 has a creep rupture life of 964 hours, while UM-F20 has a creep rupture life of 493 hours at 950°C and 290 MPa. The creep rupture life at these conditions for UM-F30 should be much greater than 1000 hours. For comparison purposes, the rupture life of CMSX-4 at 950°C and 290 MPa is 446 hours [16].

Table II. Precipitate Morphology, Volume Fraction γ' and Rafting Direction of Single Crystal Experimental Ru-Containing Nickel-Base Superalloys

Alloy	Dendrite Core			Interdendritic Region		
	γ' Precipitate Morphology	γ' Vol. Fraction	Rafting Direction	γ' Precipitate Morphology	γ' Vol. Fraction	Rafting Direction
UM-F9	Spherical	0.48	None	Intermediate	0.57	Parallel
UM-F11	Spherical	0.50	None	Spherical	0.53	None
UM-F16	Cuboidal	0.56	Perpendicular	Cuboidal	0.64	Perpendicular
UM-F18	Intermediate	0.50	Parallel	Intermediate	0.58	Parallel
UM-F19	Cuboidal	0.57	Perpendicular	Cuboidal	0.63	Perpendicular
UM-F20	Cuboidal	0.60	Perpendicular	Cuboidal	0.69	Perpendicular
UM-F22	Intermediate	0.55	Perpendicular	Intermediate	0.58	Perpendicular
UM-F27	Cuboidal		Perpendicular	Cuboidal		Perpendicular
UM-F30	Cuboidal	0.67	Perpendicular	Cuboidal	0.69	Perpendicular

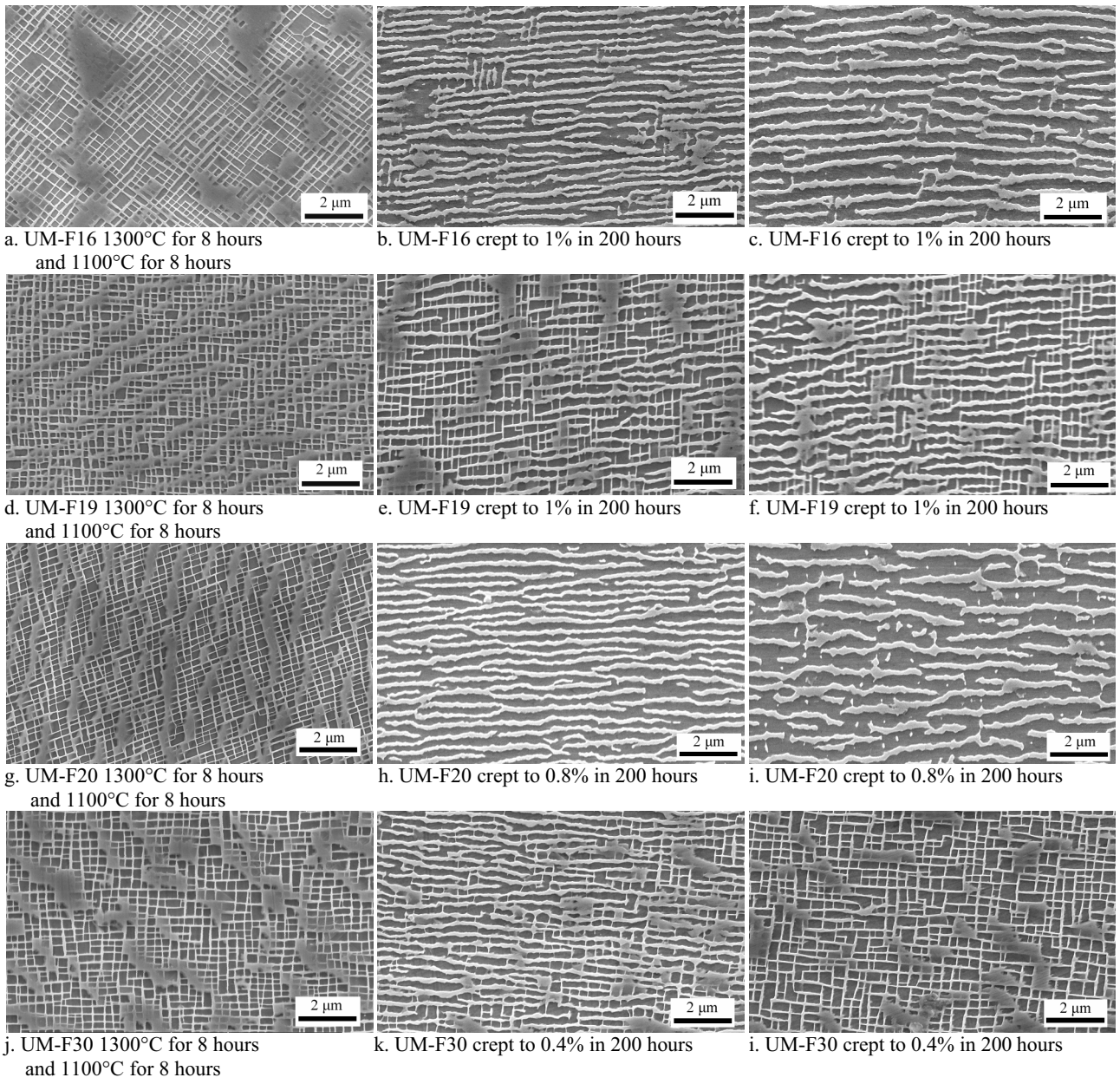

Figure 1. Left column: Solution treated and aged γ-γ' microstructure of UM-F16 (a), UM-F19 (d), UM-F20 (g), and UM-F30 (j) alloys with a cuboidal γ' precipitate morphologies. Center and right column: Post-crept γ-γ' microstructure of UM-F16 (b, c), UM-F19 (e, f), UM-F20 (h, i), and UM-F30 (k, i) alloys after creep at 950°C and 290 MPa. Applied tensile stress is in the vertical direction.

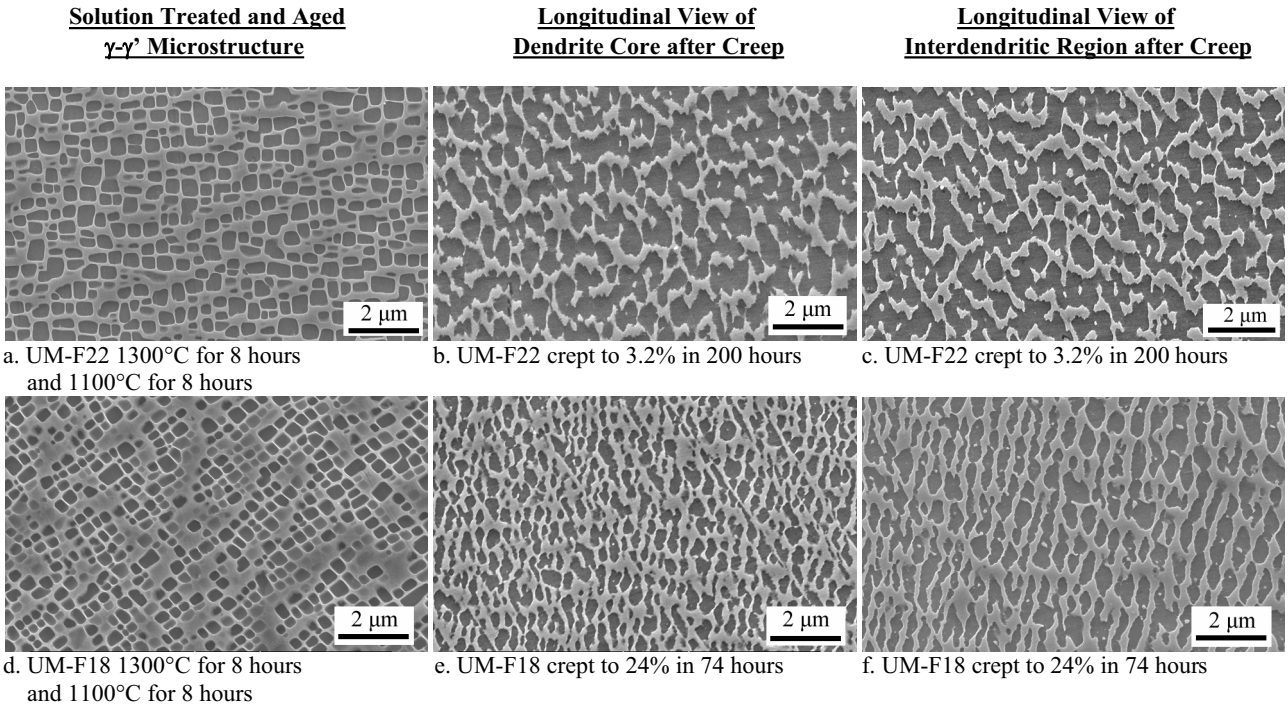

Figure 2. Left column: Solution treated and aged γ-γ' microstructure of UM-F22 (a) and UM-F18 (d) alloys with a intermediately-shaped γ' precipitates. Center and right column: Post-crept γ-γ' microstructure of UM-F22 (b, c) and UM-F18 (e, f) alloys after creep at 950°C and 290 MPa. Applied tensile stress is in the vertical column.

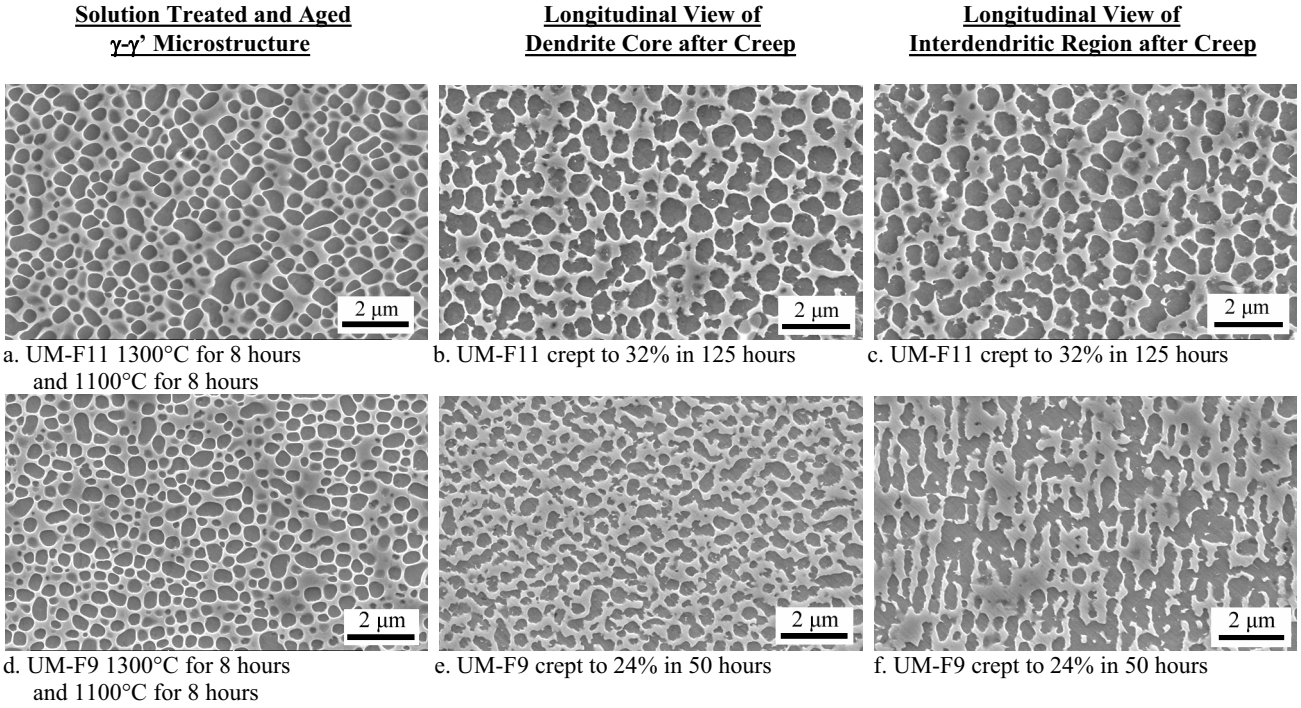

Figure 3. Left column: Solution treated and aged γ-γ' microstructure of UM-F11 (a) and UM-F9 (d) alloys with spherical γ' precipitates. Center and right column: Post-crept γ-γ' microstructure of UM-F11 (b, c) and UM-F9 (e, f) alloys after creep at 950°C and 290 MPa. Applied stress is in the vertical direction.

SEM images of the post-crept γ-γ' microstructures are shown in the right hand column of Figures 1, 2, and 3. The alloys with cuboidal precipitates rafted perpendicular to the stress axis, as expected in comparison to commercial nickel-base single crystal superalloys. The UM-F19 and UM-F30 alloys had not completely rafted after 200 hours at 290 MPa and 950°C, indicating that the rafting kinetics of these alloys are slow. Vertical γ-γ' interfaces remain in the alloys that have not completely rafted (Figures 1b, c, e, f). No vertical γ-γ' interfaces were observed in the UM-F16 (Figure 1b, c) or the UM-F20 alloy (Figure 1h, i), nor an MK-4 specimen [17] (a modified CMSX-4) after a 200 hour creep test at 950°C and 290 MPa. The compositions of UM-F20, UM-F19 and UM-F30 differ in Co content, 2.5 at%, 7.5 at%, and 10 at% respectively.

The alloys with intermediately-shaped γ' precipitates coarsened in different directions relative to the applied stress during high temperature deformation. The UM-F18 alloy crept to failure (24% in 74 hours) rafted parallel to the applied stress axis (Figure 2e, f). Coarsening of the γ' precipitates occurred perpendicular to the stress axis in the UM-F22 alloy (Figure 2b, c). It should be noted that there was no difference in the γ-γ' microstructure of the solution and aged samples and the button head of the creep specimens after creep deformation at 950°C, indicating limited coarsening under elastic conditions.

Rafting was not observed in either of the alloys with spherical γ' precipitates (Figures 3b, e). The UM-F9 alloy crept to a 0.8% creep strain in 8 hours and to failure with 22% creep strain in 50 hours (Figure 3d), did not exhibit rafting in either condition in the dendrite core. However, in the interdendritic region, the precipitates appeared to have coarsened slightly in a direction parallel to the applied stress (Figure 3f). There was no directional coarsening of the precipitates in the UM-F11 alloy crept to failure in 125 hours. The post-crept γ-γ' microstructure of UM-F11 is shown in Figure 3b and c.

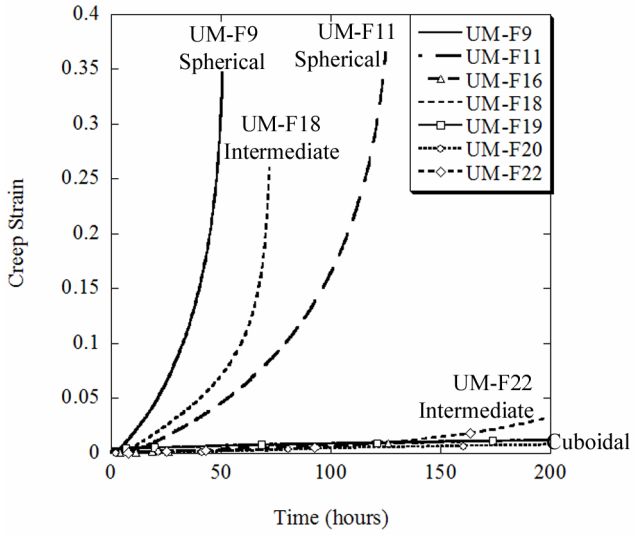

Figure 4. Creep behavior of selected experimental Ru-containing superalloys at 950°C and 290 MPa for 200 hours. Precipitate morphology is included below alloy name.

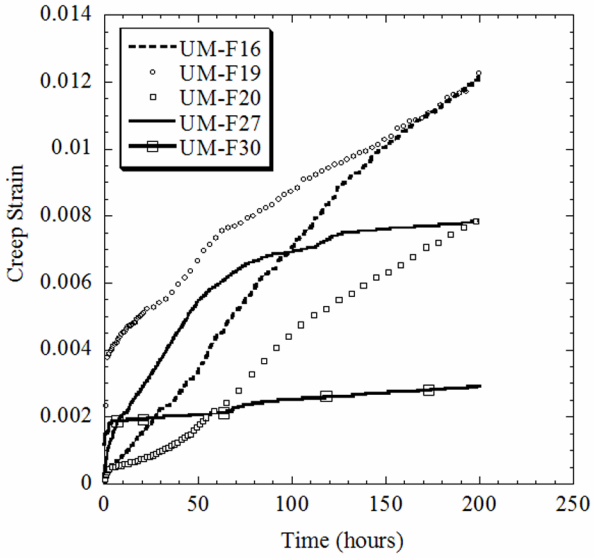

Figure 5. Creep behavior of UM-F16, UM-F19, UM-F20, UM-F27 and UM-F30 at 290 MPa and 950°C for 200 hours.

Dislocation Substructures

TEM images revealed drastically different dislocation substructures in UM-F9 (spherical γ' precipitates) and UM-F20 (cuboidal γ' precipitates) after approximately 1% creep deformation. After straining to approximately 0.8% in 200 hours, the UM-F20 alloy had a well-developed dislocation network at the γ-γ' interfaces (Figure 8). Dislocations of six-types of <110> Burgers vectors were observed. Figure 9 is a schematic of the type of dislocation network observed in the imaged area. The hexagonal dislocation network consists of three types of <110> dislocations: $<01\bar{1}>$, $<\bar{1}\,01>$, and $<1\bar{1}0>$. No dislocations appear

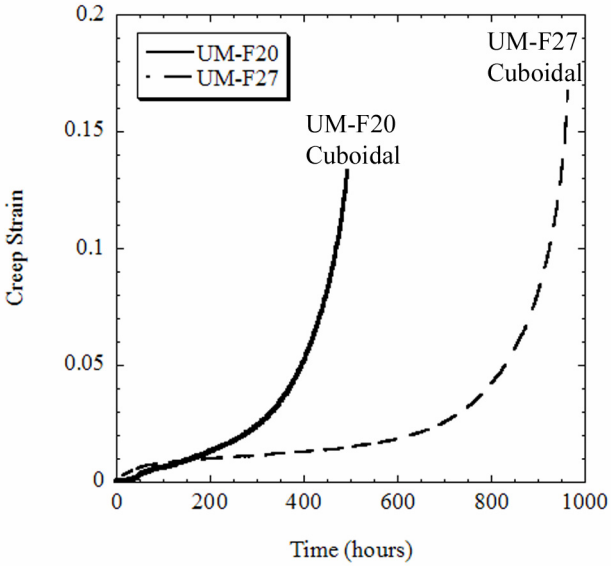

Figure 6. Creep rupture behavior of selected experimental alloys at 950°C and 290 MPa. Precipitate morphology is included below the alloy name.

to have sheared the γ' precipitates. The dislocation substructure of the UM-F20 alloy is consistent with that reported for a number of commercial nickel-base superalloys [11, 12, 18, 19].

Interestingly, an interfacial dislocation network was not observed in the UM-F9 alloy after 0.6% strain in 4 hours (Figure 9). The dislocation segments in the matrix channels were longer than those observed in UM-F20 and the overall dislocation density was much lower. Again, all six types of <110> dislocations were observed and there was no evidence of dislocations shearing the γ' precipitates.

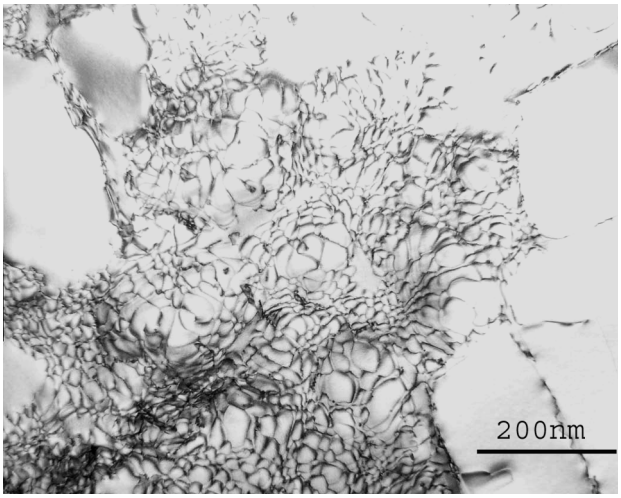

Figure 7. Dislocation substructure of UM-F20 after 0.8% creep strain at 950°C and 290 MPa.

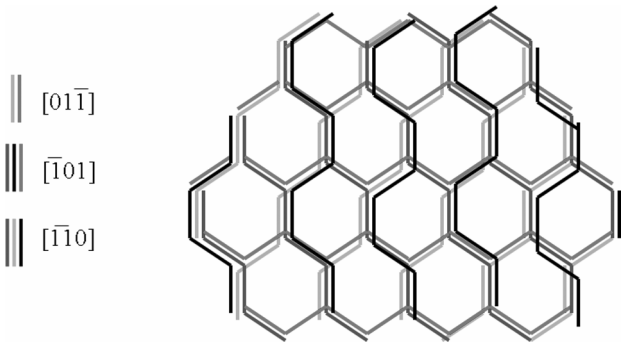

Figure 8. Idealized dislocation network observed in UM-F20 after 0.8% creep strain at 950°C and 290 MPa.

Discussion

Precipitate Morphology and γ-γ' Lattice Misfit

As mentioned previously, it is well known that the lattice misfit, the precipitate morphology, and the γ-γ' chemistry are interrelated. The chemistry controls the sign and magnitude of lattice misfit, which determines the precipitate morphology and the directional coarsening behavior during creep.

Current commercial superalloys have a negative lattice misfit because of the strong partitioning behavior of W, Re and Mo. It is also known that the direction of precipitate coarsening is dependent on the direction of the applied stress and the sign of the misfit [20, 21]. Nickel-base superalloys that raft perpendicular to the applied tensile stress axis have a negative γ-γ' lattice misfit. Alloys with a positive lattice misfit raft parallel to the applied stress. The lattice misfit is the driving force for rafting and therefore if the misfit is eliminated, then the precipitates should not directionally coarsen.

The precipitates are spherical in UM-F9 and UM-F11, which both have 9.6 wt% Ru and no Cr. Cuboidal precipitates are observed in UM-F16, UM-F19, UM-F20, UM-F27 and UM-F30, which all have 5.7 wt% Ru and 6.7 wt% Cr. The alloys with intermediate-shaped precipitates, UM-F18 and UM-F22 have 5.7 wt% Ru and no Cr and 5.7 wt% Ru and 3.4 wt% Cr, respectively. The combined Ru and Cr contents in the present set of alloys appear to strongly influence the precipitate morphology and therefore the lattice misfit and the phase compositions. Within this set of alloys, variations in the other elemental additions do not seem to have a strong effect on the precipitate shape.

The directional coarsening behavior of the alloys UM-F16, UM-F19, UM-F20, UM-F22 and UM-F30 (Figure 1), suggest a negative γ-γ' lattice misfit at the test temperature. The irregular rafts observed in UM-F22 can possibly be attributed to the fact the specimen has reached the tertiary creep regime [22]. The UM-F18 alloy rafted parallel to the applied stress, indicative of a positive misfit at 950°C. The absence of rafting in UM-F9 and UM-F11 suggest that the lattice misfit at 950°C is near-zero, and thus the lattice parameter of the γ' precipitate is nearly equal to the lattice parameter of the matrix. The variation in the γ-γ' lattice misfit in this series of alloys is surprising considering the consistent levels of Re and W additions. Again, this is likely to be due to Ru and Cr interactions and their influence on phase compositions.

The spherical γ' precipitates in UM-F9 and UM-F11 were morphologically stable during high temperature deformation. The ability to design a coarsening-resistant Re- containing superalloy with a near-zero misfit may be beneficial for certain turbine applications. Though the experimental alloys with spherical precipitates are not as creep resistant, they may be beneficial in applications that require the mechanical properties of a material to remain constant over very long periods of time.

In this set of alloys both Ru and Cr appear to influence

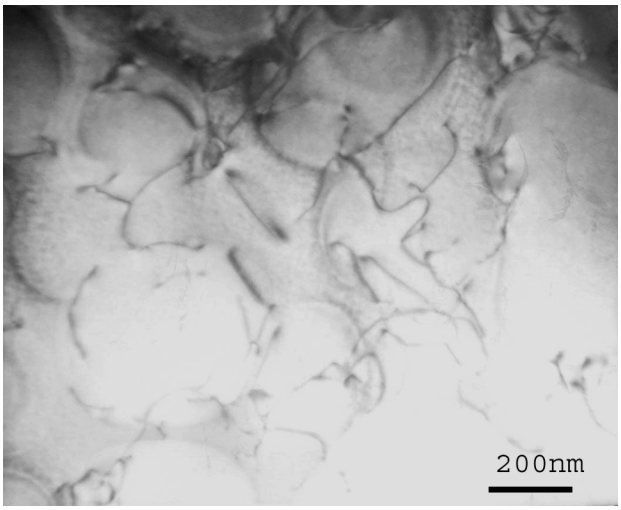

Figure 9. Dislocation substructure of the UM-F9 alloy after 0.6% strain in 4 hours at 290 MPa and 950°C.

Table III. Compositions of Commercial Nickel-Base Single Crystal Superalloys (wt%)

Alloy	Ni	Al	Ta	Re	W	Co	Cr	Ti	Mo	Hf
CMSX-4	Bal.	5.7	6.5	2.9	6.3	9.5	6.4	1.0	0.6	0.1
PWA 1484	Bal.	5.6	8.7	3.0	6.0	10.0	5.0		2.0	0.1
René N5	Bal.	6.2	6.5	3.0	5.0	7.5	6.5		1.5	0.15

partitioning and therefore misfit. Chromium, with an atomic radius very close to that of Ni, is not expected to have a strong influence on the lattice parameters of either the γ or γ' phases. Thus it is more likely that there is a strong thermodynamic interaction between Cr and Ru in the two phases, resulting in changes in partitioning of these and other refractory constituents. O'Hara and coworkers found that Ru caused Re and W to partition less strongly to the matrix [3]. The claim of less severe partitioning of Re and W to the γ as a result of Ru additions is consistent with observations on the present set of experimental alloys. The UM-F9, UM-F11 and UMF18 alloys have significant amounts of Re and W, which generally cause a more negative lattice mismatch. On the contrary, Murakami and coworkers [1] and Yokokawa and coworkers [15] found that 1.46 wt% Ru did not affect the γ-γ' partitioning behavior in TMS-75. The larger Ru additions in the experimental alloys of this study may explain the seemingly different results. Further detailed analyses of the compositions of the phases in these alloys are needed to clarify individual effects of Cr and Ru on partitioning. It is interesting to note that Smith reported a strong effect of Cr on Re partitioning in Ni-Al-Re, Ni-Al-Cr, and Ni-Al-Re-Cr alloys [23]. Using energy dispersive spectroscopy (EDS), it was determined that Re did not preferentially partition to the γ in the absence of Cr. However, the presence of Cr caused Re to strongly partition to the γ phase. A similar effect of Cr on portioning may occur within the set of alloys investigated here.

Creep Behavior

To understand creep strengths of the experimental alloys it is important to consider overall compositional variations. The amount of Co and Cr in the alloys varied significantly and the Ta contents ranged from 6.5 and 8.1 wt%. There were two levels of Ru additions in the alloys; 5.7 wt% and 9.6 wt%. As mentioned before, similar amounts of refractory elements were present in all the alloys, with a total amount of Re and W of 7.5 to 8.3 wt%. Based on the similar amounts of refractory elements in these alloys, qualitative comparisons between the creep strengths of the experimental alloys are justified.

The most obvious factor influencing creep strength in the alloys studied here is the volume fraction of γ'. Following the method used by Pollock and Argon [24], a rough calculation can be performed for comparison of the creep rate at two different volume fraction of γ' precipitates. The resistance to Orowan bowing of precipitates accounts for the majority of the creep resistance of single crystal nickel-base superalloys. For this reason the creep strength should be proportional to Gb/h, where G is the shear modulus, b is the magnitude of the Burgers vector, and h is the width of the matrix channel. Using the volume fraction of γ' reported in Table I and an average precipitate diameter of 0.4 μm, changes in creep strength due to changes in volume fraction of γ' can be estimated. The alloys UM-F11, UM-F20, and UM-F30 have approximately 0.5, 0.6 and 0.7 volume fraction of γ' precipitates, respectively. Typical values for the shear modulus and Burgers vector for this class of materials are 50 GPa and 0.254 nm, respectively. The UM-F11 alloy has 0.5 volume fraction of γ' and therefore the average channel width is estimated to be 0.1 μm. Following similar calculations for UM-F20 (0.6 volume fraction γ') and UM-F30 (0.7 volume fraction γ') estimates for the channel widths are 0.075 μm and 0.05 μm, respectively. Thus the resolved shear stress for the alloys with 0.5, 0.6 and 0.7 volume fraction of γ' precipitates is 122 MPa, 169 MPa and 254 MPa, respectively. Using the Schmid factor for [001]-oriented single crystals, the applied uniaxial stress to cause glide through the matrix channels would be 299 MPa, 415 MPa and 622 MPa, respectively. This corresponds to an order of magnitude decrease in creep rate as the volume fraction of γ' increases from 0.5 to 0.6 to 0.7; assuming the creep rate is proportional to σ^n, with n≈7 [24]. The experimental results generally scale with this estimate of difference in creep rates based solely on the volume fraction of γ' precipitates. At 290 MPa and 950°C the minimum creep rate of UM-F30 was 10^{-10}/sec, an order of magnitude less than the minimum creep rate of UM-F20, 10^{-9}/sec. The minimum creep rate of UM-F11 was approximately 10^{-8}/sec.

It is also interesting to compare the UM-F18 alloy and the UM-F11 alloy. The UM-F11 alloy has 9.7 wt% Ru and the UM-F18 alloy has 5.7 wt% Ru; neither alloy has Cr. Both alloys have 0.5 volume fraction of γ' precipitates, yet based on rafting behavior, the lattice misfit in UM-F18 is positive while the lattice misfit in UM-F11 is very near zero. Again, the higher level of Ta in the UM-F18 alloy may explain the smaller difference in the lattice parameter of the γ and the γ' and the lower creep strength of the UM-F18 alloy can most likely be attributed either to the rafting occurring parallel to the applied stress axis or to the slightly lower volume fraction of γ' precipitates. Nevertheless, it does not appear that there is a direct benefit of the addition of 4 wt% Ru to the creep strength.

Nathal and Ebert reported that higher Co contents decrease the γ' coarsening rate under an applied stress [25]. The only compositional variation in the UM-F19, UM-F20 and UM-F30 alloys was the Co content, which was 7.2, 2.4 and 10 wt%, respectively. After the aging treatment of 1100°C for 8 hours, all three alloys had a similar γ' size. However, the UM-F19 and the UM-F30 (Figure 1d, h) alloys rafted much slower than in the UM-F20 alloy (Figure 1f). The UM-F20 alloys had no vertical γ-γ' interfaces remaining in the post-crept microstructure, while there was incomplete rafting in both UM-F19 and UM-F30. It is also interesting to note that UM-F30 is significantly more creep resistant than any of the other alloys including UM-F19 and UM-F20 (Figure 5). These observations collectively suggest that Co may reduce the rate of interdiffusion in these alloys.

Finally, a Larson Miller plot was used to compare the creep rupture behavior of commercial superalloys to the Ru-containing experimental superalloys. René N5, CMSX-4, and PWA-1484 were used for comparison since they have similar levels of refractory content as the experimental alloys. The Ru-containing superalloys, UM-F20 and UM-F27 had improved temperature and stress capabilities at 950°C compared to current commercial alloys with similar refractory element content. However, it should be emphasized that the benefits of Ru additions are indirect and

arise due to interaction of Ru with other alloy constituents, resulting in a significant change in phase compositions, misfits, volume fractions and morphology. These collective changes can improve creep properties at 950°C. Further, creep tests at 1100°C are underway.

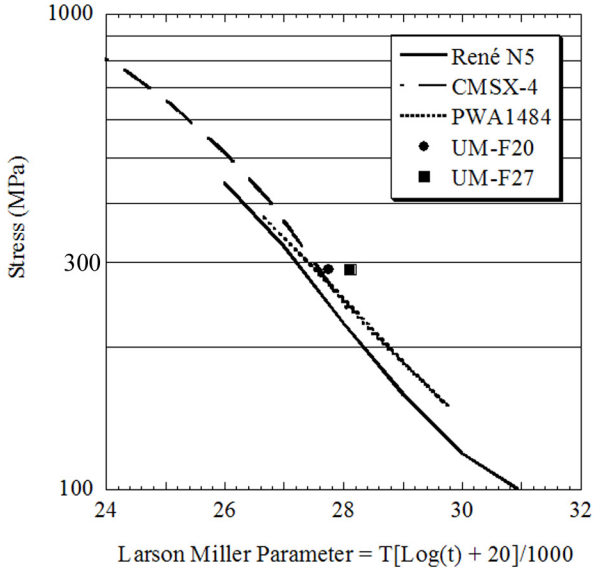

Figure 10. Larson Miller plot comparing the creep rupture strengths of the experimental alloys to commercial alloys. Larson Miller curves of commercial alloys were plotted with data from Schneider et al [16] and Duhl and Cetel [26] and Walston et al [27].

Conclusions

1. Variations in Ru and Cr additions permit a wide variety of precipitate morphologies in high refractory content single crystals to be established with positive, negative or near-zero misfit.
2. Ruthenium additions can result in improvements in creep strength at 950°C. However, the mechanisms by which Ru improves properties are indirect and require a detailed understanding of the phase equilibria.
3. The creep strengths of the experimental alloys scale with the volume fraction of γ' precipitates.

Acknowledgements

The authors are grateful for the support of the National Science Foundation, Alstom Power and the Air Force Research Laboratory.

References

1. H. Murakami, T. Honma, Y. Koizumi, and H. Harada, "Distribution of Platinum Group Metals in Ni-Base Single-Crystal Superalloys," *Superalloys 2000*, ed. T.M. Pollock, R.D. Kissinger, et al. (Seven Springs, PA: The Minerals, Metals, & Materials Society, 2000), 747-756.

2. Q. Feng, T.K. Nandy, S. Tin, and T.M. Pollock, "Solidification of High-Refractory Ruthenium-Containing Superalloys," *Acta Materialia*, 51 (2003), 269-284.

3. K.S. O'Hara, W.S. Walston, E.W. Ross, and R. Darolia, General Electric Company, US Patent #5,482,789, (1996).

4. P. Caron, "High γ' Solvus New Generation Nickel-Based Superalloys for Single Crystal Turbine Blade Applications," *Superalloys 2000*, ed. T.M. Pollock, R.D. Kissinger, et al. (Seven Springs, PA: The Minerals, Metals, & Materials Society, 2000), 737-746.

5. A.C. Yeh and S. Tin, "Solidification and Phase Stability of Ru-Bearing Ni-Base Superalloys," *Parsons 2003: Engineering Issues in Turbine Machinery, Power Plant and Renewables*, ed. A. Strang, R.D. Conroy, et al. (Trinity College Dublin, Ireland: The Minerals, Metals, & Materials Society, 2003), 673-686.

6. J.X. Zhang, T. Murakumo, H. Harada, and Y. Koizumi, "Dependence of Creep Strength on the Interfacial Dislocations in a Fourth Gernation SC Superalloy TMS-183," *Scripta Materialia*, 48 (2003), 287-293.

7. A.F. Giamei and D.L. Anton, "Rhenium Additions to a Ni-Base Superalloy: Effects on Microstructure," *Metallurgical Transactions A*, 16A (1989), 1997-2005.

8. M.V. Nathal, R.A. Mackay, and R.G. Garlick, "Temperature Dependence of γ–γ' Lattice Mismatch in Nickel-Base Superalloys," *Materials Science and Engineering*, 75 (1985), 195-205.

9. R.A. MacKay, M.V. Nathal, and D.D. Pearson, "Influence of Molybdenum on the Creep Properties of Nickel-Base Superalloy Single Crystals," *Metallurgical Transactions A*, 21A (1990), 381-388.

10. T.M. Pollock and A.S. Argon, "Creep Resistance of CMSX-3 Nickel Base Superalloy Single Crystals," *Acta Metallurgica et Materialia*, 40 (1) (1992), 1-30.

11. T.P. Gabb, S.L. Draper, D.R. Hull, R.A. MacKay, and M.V. Nathal, "The Role of Interfacial Dislocation Networks in High Temperature Creep of Superalloys," *Materials Science and Engineering*, A118 (1989), 59-69.

12. T.M. Pollock and R.D. Field. "Dislocations and High-Temperature Plastic Deformation of Superalloy Single Crystals," *Dislocation in Solids*, vol. 11 ed. F.R.N. Nabarro and M.S. Duesbery, (Amsterdam, Netherlands: Elsevier Science B.V., 2002), 593-595.

13. M. Fährmann, P. Fratz, O. Paris, E. Fährmann, and W.C. Johnson, "Influence of Coherency Stress on Microstructural Evolution in Model Ni-Al-Mo Alloys," *Acta Metallurgica et Materialia*, 43 (3) (1995), 1007-1022.

14. Q. Feng, T.K. Nandy, L.J. Rowland, B. Tryon, D. Banerjee, and T.M. Pollock, ""New Phases in Ruthenium-Containing Single Crystal Superalloys"," *Superalloys 2004*, ed.

(Seven Springs, PA: The Minerals, Metals, & Materials Society, 2004),

15. T. Yokokawa, M. Osawa, K. Nishida, T. Kobayashi, Y. Koizumi, and H. Harada, "Partitioning Behavior of Platinum Group Metals on the γ and γ' phases of Ni-Base Superalloys at High Temperatures," *Scripta Materialia*, 49 (2003), 1041-1046.

16. W. Schneider, J. Hammer, and H. Mughrabi, "Creep Deformation and Rupture Behaviour of the Monocrystalline Superalloy CMSX-4 - A Comparison with the Alloy SRR 99," *Superalloys 1992*, ed. S.D. Antolovich, R.W. Stusrud, et al. (Seven Springs, PA: The Minerals, Metals, & Materials Society, 1992), 589-598.

17. M. Konter, M. Newnham, and C. Tonnes, ABB Research Ltd., U.S. Patent #5,759,301, (1998).

18. R.R. Keller, H.J. Maier, and H. Mughrabi, "Characterization of Interfacial Dislocation Networks in a Creep-Deformed Nickel-Base Superalloy," *Scripta Metallurgica et Materialia*, 28 (1993), 23-28.

19. D.F. Lahrmann, R.D. Field, R. Darolia, and H.L. Fraser, "Investigation of Techniques for Measuring Lattice Mismatch in a Rhenium Containing Nickel Base Superalloys," *Acta Metallurgica*, 36 (5) (1988), 1309-1320.

20. M. Fährmann, W. Hermann, E. Fährmann, A. Boegli, T.M. Pollock, and H.G. Sockel, "Determination of Matrix and Precipitate Elastic Constants in (γ–γ') Ni-Base Model Alloys, and Their Relevance to Rafting," *Materials Science and Engineering A*, 260 (1999), 212-221.

21. A. Fredholm and J.L. Strudel, "On The Creep Resitance of Some Nickel Base Single Crystals," *Superalloys 1984*, ed. M. Gell, C. Kortovich, et al. (Seven Springs, PA: The Minerals, Metals, & Materials Society, 1984), 211-220.

22. M.V. Nathal and L.J. Ebert, "Gamma Prime Shape Changes During Creep of a Nickel-Base Superalloy," *Scripta Metallurgica*, 17 (1983), 1151-1154.

23. J. Smith, "Effects of Cr and Re Additions Upon Coarsening and Deformation Behavior of Single-Crystal Ni-Base Model Superalloys," (Ph.D thesis, University of Illinois at Urbana-Champaign, 1987), 88-115.

24. T.M. Pollock and A.S. Argon, "Intermediate Temperature Creep Deformation in CMSX-3 Single Crystals," *Superalloys 1988*, ed. S. Reichman, D.N. Duhl, et al. (Seven Springs, PA: The Minerals, Metals, & Materials Society, 1988),

25. M.V. Nathal and L.J. Ebert, "The Influence of Cobalt, Tantalum, and Tungsten on the Microstructure of Single Crystal Nickel-Base Superalloys," *Metallurgical Transactions A* (16A) (1985), 1849-1862.

26. D.N. Duhl and A.D. Cetel, United Technologies Corporation, Advanced High Strength Single Crystal Superalloy Compositions, (1988).

27. W.S. Walston, K.S. O'Hara, E.W. Ross, T.M. Pollock, and W.H. Murphy, "René N6: Third Generation Single Crystal Superalloy," *Superalloys 1996*, ed. R.D. Kissinger, D.J. Deye, et al. (Seven Springs, PA: The Minerals, Metals, & Materials Society, 1996), 27-34.